AGU PUBLICATIONS

Geophysical Research Letters

RESEARCH LETTER
10.1002/2015GL065175

Key Points:
- We show a unified model for stability of gravel and sand bed river bifurcations
- We predict that the majority of symmetrical river bifurcations on Earth are unstable
- Our results are favorably supported by observations

Correspondence to:
M. Bolla Pittaluga,
michele.bollapittaluga@unige.it

Citation:
Bolla Pittaluga, M., G. Coco, and M. G. Kleinhans (2015), A unified framework for stability of channel bifurcations in gravel and sand fluvial systems, *Geophys. Res. Lett.*, *42*, 7521–7536, doi:10.1002/2015GL065175.

Received 1 JUL 2015
Accepted 18 AUG 2015
Accepted article online 24 AUG 2015
Published online 16 SEP 2015

A unified framework for stability of channel bifurcations in gravel and sand fluvial systems

Michele Bolla Pittaluga[1], Giovanni Coco[2], and Maarten G. Kleinhans[3]

[1]Department of Civil, Chemical and Environmental Engineering, University of Genoa, Genoa, Italy, [2]School of Environment, University of Auckland, Auckland, New Zealand, [3]Faculty of Geosciences, Universiteit Utrecht, Utrecht, Netherlands

Abstract Bifurcating rivers shape natural landscapes by distributing water and sediments on fluvial plains and in deltas. Symmetrical bifurcations were often found to be unstable so that one branch downstream of the bifurcation enlarged while the other dwindled. A unified theory able to predict bifurcation stability in both gravel bed and sand bed rivers is still lacking. Here we develop a new theory for the stability of bifurcations for the entire range of gravel bed to sand bed rivers. The theory indicates opposite behavior of gravel bed and sand bed rivers: we predict that symmetrical bifurcations are inherently stable for intermediate Shields stresses but are inherently unstable for the low and high Shields stresses found in the majority of rivers on Earth. In the latter conditions asymmetrical bifurcations are stable. These predictions are corroborated by observations and have ramifications for many environmental problems in fluviodeltaic settings.

1. Introduction

Bifurcations are ubiquitous features of fluviodeltaic landscapes. Their presence and morphodynamic evolution shapes and alters flow and sediment redistribution over entire fluvial plains and deltas [*Edmonds and Slingerland*, 2008; *Makaske*, 2001; *Slingerland and Smith*, 2004; *Kleinhans et al.*, 2013]. River bifurcations are a major feature of both gravel bed and sand bed rivers and have been observed to be unstable over timescales ranging from decades to millennia [*Slingerland and Smith*, 2004; *Kleinhans et al.*, 2008, 2011]. New bifurcations continue to form new pathways for water and sediment that may cause avulsion, i.e., entire river displacement [*Makaske*, 2001; *Slingerland and Smith*, 1998; *Kleinhans et al.*, 2010]. Hence, stability and development of bifurcations can lead to natural hazards and land loss as well as land gain, which threaten and impact societies and valuable ecological habitats on fluvial plains and deltas [*Syvitski and Saito*, 2007]. For all the above reasons, the stability of bifurcations has been a topic of research interest over the past few decades, and significant advances have been achieved (see *Kleinhans et al.* [2013] for a review). The puzzling aspect of river bifurcations is that rather than evolving toward a configuration where flow and sediment transport are equally divided in the two branches, they almost inevitably develop asymmetric configurations with differential transport rates, in both gravel bed and sand bed rivers.

Following the pioneering studies of *Slingerland and Smith* [1998] and *Wang et al.* [1995], *Bolla Pittaluga et al.* [2003] provided a first systematic study of gravel bed river bifurcations. Using a simple model relating the flow and the sediment transport in the channels through a nodal relationship upstream of the bifurcation, *Bolla Pittaluga et al.* [2003] found that for low values of the Shields parameter typical of gravel bed rivers with dominant bed load sediment transport, symmetrical bifurcations are unstable and can result in two other configurations with both branches open, apart from the trivial solution with exactly equal flows in both channels. However, above a threshold value of the Shields stress (about 0.1) in the channel upstream of the bifurcation the model predicts only one possible stable solution which may be symmetrical. Model predictions were experimentally tested [*Bertoldi and Tubino*, 2007], and further model developments [e.g., *Miori et al.*, 2006, 2012; *Sloff and Mosselman*, 2012; *Kleinhans et al.*, 2012, *van der Mark and Mosselman*, 2013] included additional factors, for example, channels with erodible banks or secondary currents at the node upstream of the bifurcation, without fundamentally altering the findings of *Bolla Pittaluga et al.* [2003].

The stability of bifurcations in sand bed rivers has primarily been investigated with numerical models (e.g., Delft3D), and analyses inevitably conclude that sand bed rivers also develop highly asymmetrical bifurcations [*Kleinhans et al.*, 2008; *Edmonds and Slingerland*, 2008; *Edmonds et al.*, 2010]. *Edmonds and Slingerland* [2008]

specifically attempted to develop equilibrium diagrams for cohesive deltaic bifurcations showing that for Shields values larger than 0.12 it is possible to obtain asymmetrical solutions. This tendency to asymmetrical bifurcations is evidenced by the many occurrences of avulsion and the apparent absence of stable symmetrical bifurcations [*Kleinhans et al.*, 2013]. Although a prima vista this contradicts the model predictions of *Bolla Pittaluga et al.* [2003], the latter does not include suspended sediment transport and so cannot be directly applied to sand bed rivers.

Thus, the lack of a unified model for bifurcations in gravel bed and sand bed rivers is a major gap in our understanding. Here we develop a unifying model for bifurcation stability that explicitly addresses the different sediment transport mechanisms and sensitive parameters of gravel bed and sand bed rivers. In the following sections we formulate the problem (section 2), and, after providing an analytical solution to the problem, we analyze the reason why most gravel bed and sand bed river symmetrical bifurcations are inherently unstable (sections 3 and 4). We then provide the equilibrium configurations of river bifurcations (section 5). Section 6 summarizes the main conclusions of this contribution. The full derivation is given in the appendix.

2. Model Development

Our analytical model concerns the development of bifurcating river channels after the bifurcation is initiated, which may occur through various mechanisms [*Kleinhans et al.*, 2013]. Once a bifurcation exists, one of the two flow paths will enlarge and capture more of the discharge if and only if its transport capacity exceeds the sediment supply to it. How water discharge and bed material flux are distributed across the channel immediately upstream of the bifurcation determines the division between left and right branches and the stability. We idealize bifurcations to a simple geometry (Figure 1), where a wide rectangular channel *a* bifurcates into two equiwidth channels *b* and *c*. All branches have constant width and bed slope. Constant flow and sediment discharges are prescribed upstream, whereas a constant value of free surface elevation is imposed at the downstream end in both channels *b* and *c*. In agreement with a large body of numerical and empirical work [*Kleinhans et al.*, 2012, 2013], we presume that equilibrium river morphology is predictable from a single constant discharge that is representative for a hydrological regime with low flow and floods over a longer period. For every channel the steady and uniform flow is described by the Chezy relation. The steady state and continuity conditions also imply that flow discharge Q_i and sediment flux Q_{si} are constant in each channel *i* (*b* or *c*) [*Bolla Pittaluga et al.*, 2014].

Bifurcation instability is the result of the nonlinear dependence of dimensionless sediment transport capacity [*Wang et al.*, 1995] Φ on excess dimensionless Shields number:

$$\phi = \frac{q_s}{\sqrt{\frac{\rho_s-\rho}{\rho} g d_s^3}} = n(D)(\vartheta - \vartheta_{cr})^m, \tag{1}$$

where q_s is the dimensional volumetric sediment flux per unit width, d_s is the mean diameter, ρ and ρ_s are the density of water and sediment, respectively, g is gravitational acceleration, ϑ_{cr} is the threshold value for sediment mobilization, and the coefficients n and m depend on the sediment transport closure relation. The Shields number ϑ is in turn a function of flow velocity, sediment characteristics (density and mean diameter), and the Chezy flow resistance coefficient. Classic sediment transport relations for gravel (bed load) [*Meyer-Peter and Müller*, 1948], sand (suspended load) [*Engelund and Hansen*, 1967], and the entire range [*van Rijn*, 1984] can be expressed directly in the form of equation (1) with $m = 1.5–2.5$.

Five relations are required to solve the water and sediment partitioning at the bifurcation: (1) water discharge balance $Q_a = Q_b + Q_c$; (2) and (3) constancy of water level $h_a = h_b = h_c$; and (4) and (5) sediment mass balance applied to both cells of the final reach of channel *a* (see Appendix A). The sediment balance describing the transverse sediment exchange between the two adjacent cells of the final reach of channel *a* (see Figure 1a) provides the additional relation to close the problem mathematically. Transverse sediment transport at this node depends on the transverse fluid flow and the bed slope *Ikeda et al.* [1981]:

$$q_{sy} = q_{sa}\left[\frac{V}{\sqrt{U^2+V^2}} - \frac{r}{\sqrt{\vartheta_a}}\frac{\partial \eta}{\partial y}\right], \tag{2}$$

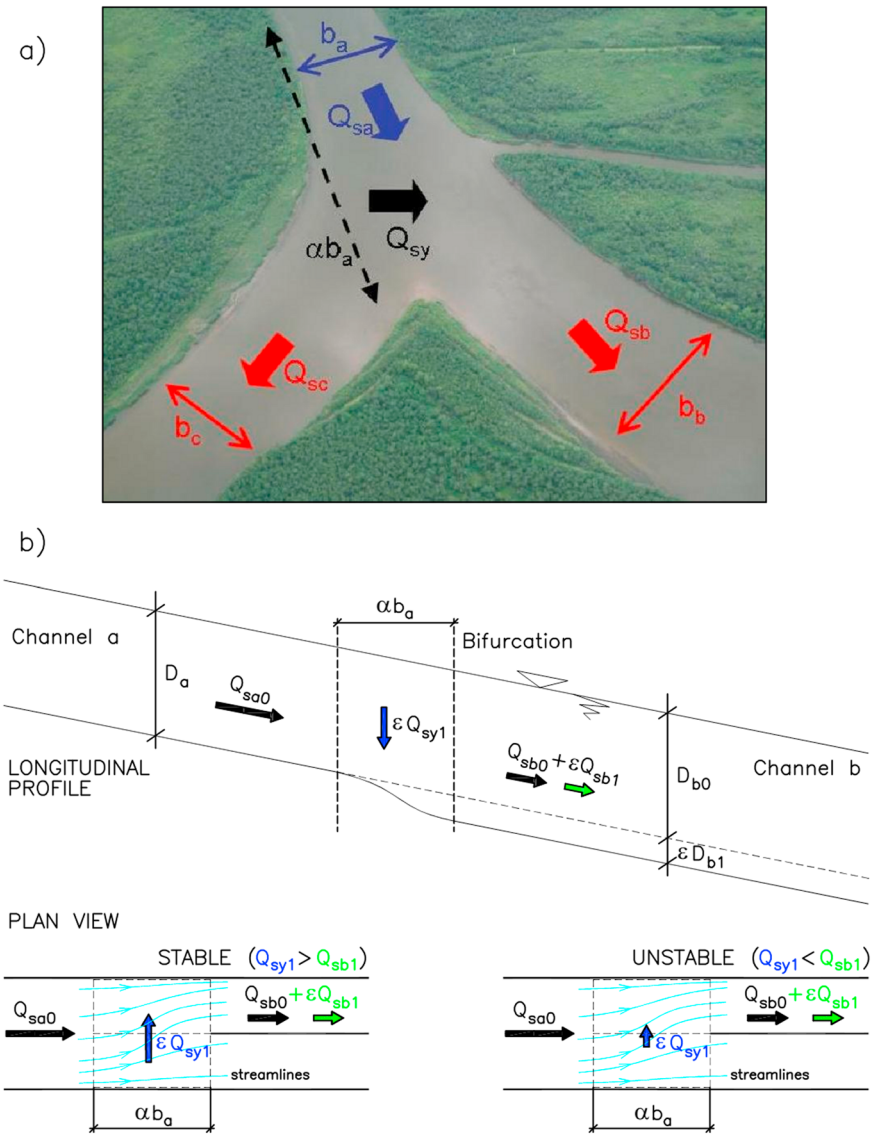

Figure 1. Geometry of a river bifurcation and cartoon of the instability process. (a) Definition sketch of sediment fluxes at a river bifurcation. The line αb_a indicates the location of transverse sediment transport. The bifurcation is in equilibrium when the sediment supply to each downstream branch equals the sediment transport capacity in that branch. (b) Sketch of the effect of the perturbation of channel depth ϵD_{b1} in channel *b* on the sediment transport capacity ϵQ_{sb1} (proportional to the r.h.s. of equation (3)) and lateral sediment transport at the bifurcation ϵQ_{sy1} (proportional to the l.h.s. of equation (3)).

where the transverse velocity *V* is evaluated through the water mass balance applied to each of the two cells [*Bolla Pittaluga et al.*, 2003]. The transverse bed slope $\partial\eta/\partial y$ is calculated from the difference between bed elevations at the inlet of channels *b* and *c* which develops as a bifurcation becomes asymmetrical [*Bolla Pittaluga et al.*, 2003]. Parameter *r* in equation (2) is uncertain and ranges between 0.3 and 1 [*Ikeda et al.*, 1981].

3. Stability Analysis of Symmetrical Bifurcations

To understand the basic mechanisms underlying bifurcation stability, let us consider an exactly symmetrical bifurcation with channel width $b_b = b_c = b_a/2$ and same downstream channel length $L_b = L_c$. In this case, a trivial solution exists where all branches have the same flow depth $D_a = D_b = D_c$, and an equal partitioning of flow and sediment fluxes occurs in the downstream branches: $Q_b = Q_c = Q_a/2$ and $Q_{sb} = Q_{sc} = Q_{sa}/2$. This equilibrium configuration is not necessarily stable to any perturbation. Indeed, consider such configuration subject to a small perturbation, here a slight increase of flow depth $D_b = D_{b0} + \epsilon D_{b1}$ along channel *b*

(Figure 1b). The consequence of this perturbation is that the sediment transport capacity in *b* increases. At the same time the larger depth in *b* creates a transverse bed slope just upstream of the bifurcation. This is directed toward channel *b* so that the sediment input into channel *b* also increases. The relative increase of the two quantities determines whether the bifurcation is stable. If the sediment transport capacity increases more rapidly than the sediment supplied from upstream, there will be more sediment leaving channel *b* than that entering the channel from upstream. This results in a positive feedback between the initial perturbation and the bed evolution that will lead to continued deepening of channel *b*. This means that the symmetrical bifurcation is unstable and should evolve into an asymmetrical bifurcation that is stable. Vice versa, if the sediment transport capacity increases less than sediment feed from the node, the channel will reduce the initial perturbation of flow depth and will converge again on the stable, symmetrical configuration.

Such qualitative description of the basic mechanism underlying stability shows that a different behavior between symmetrical bifurcation in sand bed and gravel bed rivers might exist. This has to be ascribed mainly to two factors: (1) the relation between sediment transport capacity and Shields number becoming highly nonlinear for both near-threshold Shields numbers (appropriate for gravel bed rivers) and large values of Shields number (appropriate for sand bed rivers) and (2) the stabilizing effect associated with lateral sediment transport becoming larger as Shields numbers gets smaller (i.e., in gravel bed rivers). Through perturbation analysis we derive a unifying analytical expression predicting the threshold condition for the stability of a symmetric bifurcation appropriate for both sand bed and gravel bed rivers (see Appendix A):

$$\left(\frac{3}{2}+\frac{2.5}{C_a}\right)+\frac{8\alpha r}{\beta_a\sqrt{\vartheta_a}}=m\frac{\vartheta_a}{\vartheta_a-\vartheta_{cr}}+\frac{1}{n}\frac{\mathrm{d}n}{\mathrm{d}D}\bigg|_{\epsilon=0}D_a. \tag{3}$$

This relation for the threshold condition is a function of the Shields number of the upstream channel ϑ_a, the aspect ratio β_a, the dimensionless Chezy coefficient C_a, the exponent m and the coefficient n appearing in the sediment transport law, the coefficient accounting for the transverse bed slope on sediment transport r, and the α coefficient that accounts for the upstream distance from the bifurcation where the morphological effect of the bifurcation decays *Bolla Pittaluga et al.* [2003]. The left-hand side (l.h.s.) of equation (3) is proportional to the perturbation of the transverse sediment flux at the node (ϵQ_{sy1}) which, in turn, depends upon the transverse component of flow velocity and the lateral bed slope (see equation (2)). The right-hand side (r.h.s.) of equation (3) is proportional to the perturbation of the sediment transport capacity in the downstream branches (see equation (1)). When both sides of equation (3) are equal, the so-called marginal stability configuration is attained. Under such circumstance, the initial perturbation (small increase) of flow depth in the downstream channel neither grows nor decays. The bifurcation is defined as stable when the initial perturbation reduces in time. This occurs when the l.h.s. of equation (3) (representing "sediment input") is larger than the r.h.s. (representing "carrying capacity"). In this case, indeed, more sediment is supplied to the channel that was perturbed (deepened) by the initial perturbation. This excess of sediment supply tends to decrease the flow depth damping down the initial perturbation, and the bifurcation is consequently stable. Vice versa, the bifurcation is defined as unstable when the initial perturbation grows in time. This occurs when the l.h.s. (representing sediment input) is smaller than the r.h.s. (representing carrying capacity). In this case more sediment is leaving from the channel that was deepened by the initial perturbation. This excess of sediment export from the downstream channel tends to increase the flow depth amplifying the initial perturbation, and the bifurcation is consequently unstable.

Equation (3) is plotted in Figure 2 considering the values of the coefficients n, m, and ϑ_{cr} appropriate for gravel and sand bed rivers. As stated in Appendix A, for gravel bed rivers dominated by bed load transport the Meyer-Peter and Müller relation applies ($n = 8$, $m = 1.5$, and $\vartheta_{cr} = 0.047$), so that equation (3) reduces to equation (A22). In the case of sand bed rivers dominated by suspended load transport the Engelund and Hansen relation applies ($n = 0.05C^2$, $m = 2.5$, and $\vartheta_{cr} = 0$), so that equation (3) reduces to equation (A23). For given values of C and αr, equations (A22) and (A23) represent a relation between β and ϑ that is plotted in Figure 2. Here we show again the opposite behavior of gravel bed and sand bed rivers and the agreement with the data. Given that both r and α are rather uncertain, we bracket likely the values of their product. The relation is only slightly sensitive to the value used for Chezy. To indicate the relevance of our results, we also plot histograms for Shields numbers and aspect ratios of natural sand bed and gravel bed rivers from a global data set [*Kleinhans and van den Berg*, 2011]. We excluded braided rivers from these data because these have several parallel channels whereas the analysis pertains to single channels.

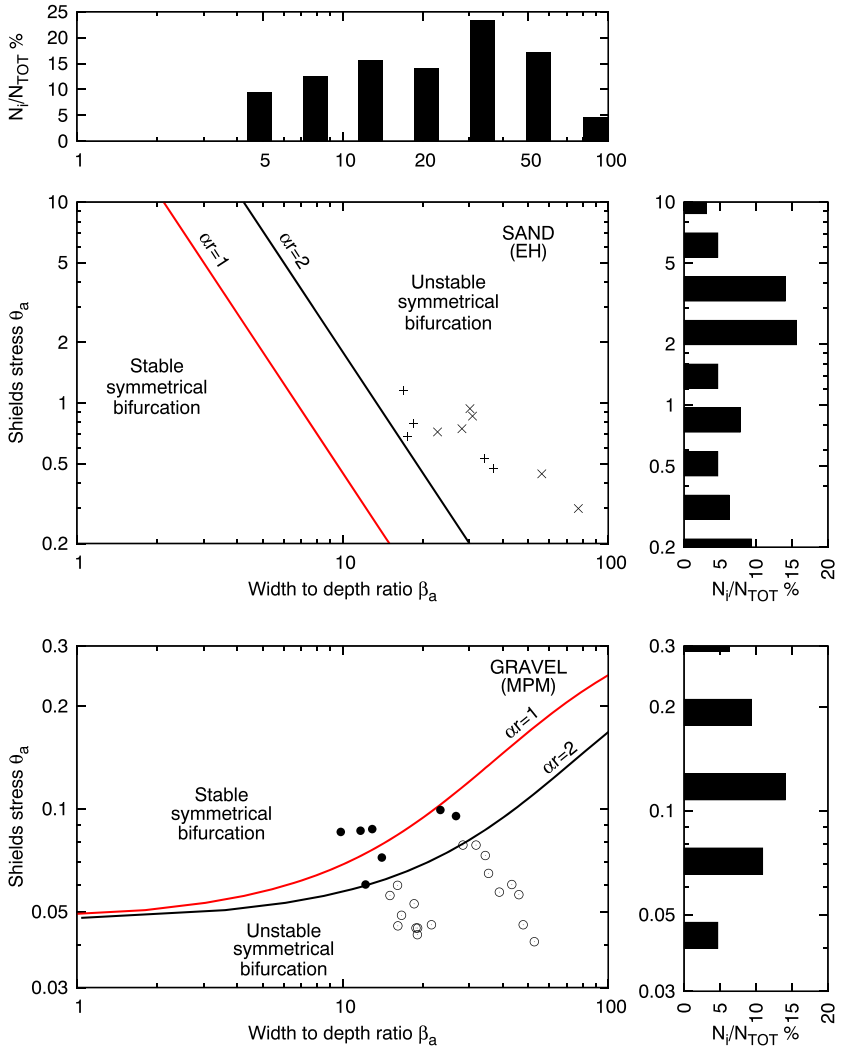

Figure 2. Stability diagram of river bifurcations. Thresholds that separate a regime where bifurcations are stable with a symmetrical configuration and a regime where symmetrical bifurcations are unstable and asymmetrical bifurcations are stable. The lines bracket likely values of the product of α and r parameters which are both uncertain. Plotted data are from Figure 3: solid circle, flume (unstable); open circle, flume (stable) [*Bertoldi and Tubino*, 2007]; cross, Cumberland Marshes this paper; and plus, Columbia River [*Kleinhans et al.*, 2012]. Histograms show a population of natural river channels [*Kleinhans and van den Berg*, 2011] indicating which regimes are likely found in nature. $C_a = 13$.

4. Physical Explanation

The striking opposite behavior of sand bed and gravel bed rivers can be clarified on the basis of equation (3) and Figure 1b. The stability of a bifurcation is mainly governed by the difference between the sediment transport capacity in the downstream branches (proportional to the r.h.s. of equation (3)) and the sediment input provided to the downstream channels from the node (proportional to the l.h.s. of equation (3)). This balance works out differently in gravel bed and sand bed rivers because of the different dependence of sediment transport capacity on the Shields number. Let us consider first the case of gravel bed rivers. Assuming a critical value of 0.047 and a Shields stress 1.4 times the critical value, the r.h.s. of equation (3) turns out to be 16.5. Considering a width-to-depth ratio $\beta = 30$, a Chezy coefficient $C = 13$, and $\alpha r = 1$, the r.h.s. of equation (3) gives 5.25, a value larger than the l.h.s. that is equal to 2.73. This is often the case in gravel bed rivers that hence show a tendency to unstable bifurcations. Indeed, in order to have r.h.s. equal to l.h.s., we should either decrease the aspect ratio to 8.8 (extremely narrow channel!) or increase the Shields number to 0.12 (corresponding to 2.6 times the critical value!) by keeping all the other parameters unchanged. Let us now consider the case of sand bed rivers. Assuming the Engelund and Hansen relation, a width-to-depth ratio $\beta = 30$, a

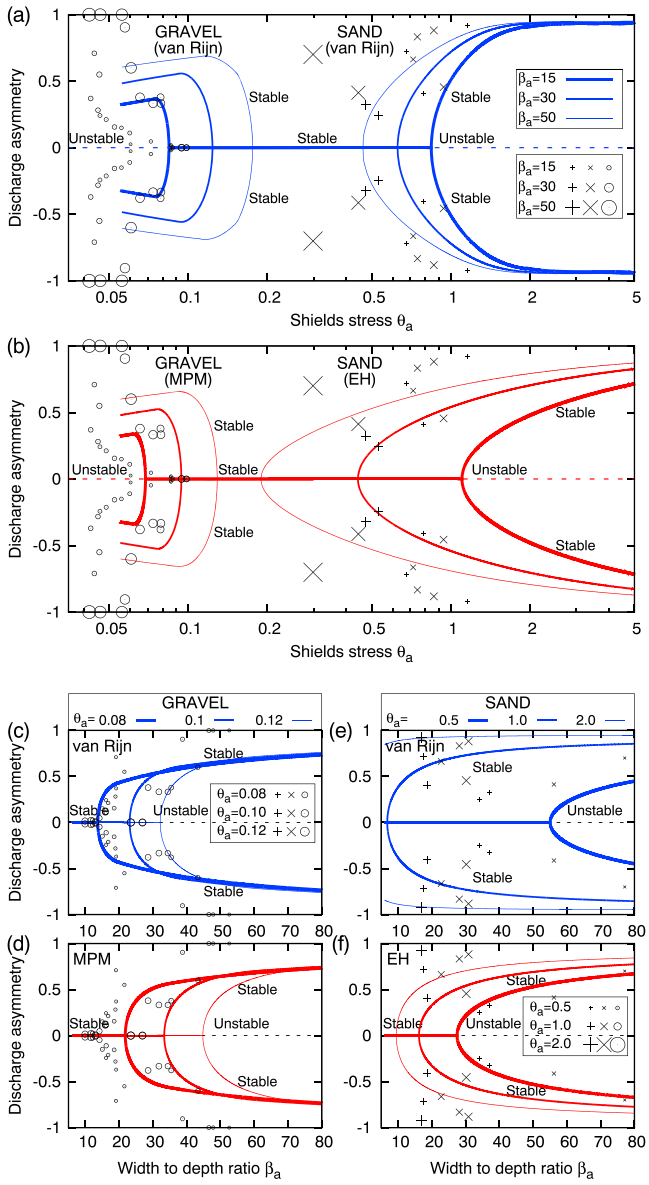

Figure 3. Equilibrium configurations of sand bed and gravel bed river bifurcations. The discharge asymmetry ΔQ is plotted versus (a and b) the Shields number ϑ_a and (c and d) the channel width-to-depth ratio β_a for the universal van Rijn sediment transport relation [*van Rijn*, 1984] (Figures 3a and 3c) and the gravel bed [*Meyer-Peter and Müller*, 1948] and sand bed [*Engelund and Hansen*, 1967] relations (Figures 3b and 3d). Continuous lines indicate stable solutions; dashed lines indicate regions were the trivial ($\Delta Q = 0$) solution is unstable. Discontinuities in Figure 3a arise from crossing the threshold to no sediment motion in the subordinate branch. We plot data of bifurcations from the following data sets: open circle, *Bertoldi and Tubino* [2007]; cross, Cumberland Marshes (M.G. Kleinhhans, unpublished); and plus, Columbia River *Kleinhans et al.* [2012]. We found no data of asymmetrical bifurcations in high mobility sand bed rivers, but numerous cases of full avulsion are known [*Makaske*, 2001; *Kleinhans et al.*, 2013]. Parameter values are $\alpha = 3$, and $r = 0.5$, $C_a = 13$.

Chezy coefficient $C = 13$, and $\alpha r = 1$, it turns out that the r.h.s. of equation (3)) is independent of the Shields number and gives 2.88. For a Shields stress ranging from 0.5 to 10, the l.h.s. gives a value ranging from 2.1 to 1.8, again lower than the r.h.s. This shows again that the vast majority of sand bed rivers are characterized by unstable symmetric bifurcations, i.e., they tend to evolve toward asymmetric configurations. For gravel bed rivers with a low Shields number close to the threshold for sediment mobility the first term on the r.h.s. of equation (3) can be extremely large. This means that a small increase of flow depth in one downstream branch implies a large increase in sediment transport capacity that cannot be balanced by the extra sediment feed at

the node due to the transverse bed slope effect. However, at higher Shields number further above the threshold for sediment motion the first term on the r.h.s. of (3) tends to $m = 1.5$. Here the l.h.s. of (3) is larger than the r.h.s. of (3) so that for higher Shields number the bifurcation is stable. In sand bed rivers with dominant suspended transport and a Shields number far above the threshold for motion, the r.h.s. of (3) is equal to the sum of a constant ($m = 2.5$) and a second term that only weakly depends on flow depth ($5/C_a$). This sum will generally be larger than the l.h.s. of (3) which is smaller for increasingly larger Shields numbers, larger aspect ratio β_a, or smaller αr.

Our physical explanation of the stability of river bifurcations is different from that provided by *Edmonds and Slingerland* [2008]. Indeed, we explain the inverse behavior of gravel bed and sand bed rivers in terms of an analytical model that helps to clarify the role of different exponents in the sediment transport relation, whereas *Edmonds and Slingerland* [2008], on the basis of a series of numerical simulations performed with Delft3D, attributed it to differential local water surface slopes at the bifurcation.

5. Equilibrium Configurations

To find equilibrium solutions, the five unknowns Q_b, Q_c, Q_{sb}, Q_{sc}, and h_a must be determined from the five nodal relations. Here we solve the full nonlinear system of equations (see Appendix A) employing a Newton-Raphson method. We span a wide range of water and sediment partitioning ratios to check for multiple equilibrium solutions. Because our main question is about the stability and symmetry of bifurcations, we report the discharge asymmetry ΔQ defined as the ratio $(Q_b - Q_c)/Q_a$.

Results show the opposite behavior of sand bed and gravel bed rivers, which explains the discrepancy between numerical model results reported until now. We find that both sand bed rivers and gravel bed rivers have a sediment mobility regime with a single stable, symmetrical solution and a regime with two stable but asymmetrical configurations (Figure 3). However, the two are opposed for gravel bed and sand bed rivers. For bifurcations in low-mobility gravel bed rivers three equilibrium solutions exist: the trivial and unstable symmetrical solution ($\Delta Q = 0$) and two stable but asymmetrical solutions. This means that symmetrical bifurcations in gravel bed rivers are unstable [*Bolla Pittaluga et al.*, 2003]. For sand bed rivers, on the other hand, we find unstable configurations *above* a threshold Shields number, meaning that most sand bed rivers cannot have stable symmetrical bifurcations. The exact thresholds for stable bifurcations depend on the chosen parameters, on the width-to-depth ratio, or aspect ratio of the upstream channel β_a, and on the chosen closure relation for sediment transport. These results are supported by the sparse field and laboratory observations of (near-) equilibrium bifurcations (Figure 3). However, given the number of uncertainties affecting both the field data and the theoretical model, the comparison must be considered more from a qualitative rather than from a quantitative point of view. The fact that for small values of the Shields stress points tend to diverge from the symmetrical equilibrium configuration is correctly predicted by the theory. Also, such tendency toward asymmetry, stronger for larger aspect ratio, is correctly predicted by the theoretical model. A similar correct qualitative behavior is shown for high values of the Shields stress corresponding to the sand region.

To summarize, this analysis shows that the majority of sand bed rivers have asymmetrical bifurcations. Nevertheless, a relatively low-sediment mobility regime exists with stable symmetrical bifurcations that may be relevant for low gradient fluvial plains and deltas particularly with low aspect ratios.

6. Conclusions

We developed a framework that predicts the stability of bifurcations in gravel bed and sand bed rivers. This stability is mostly determined by sediment mobility and channel aspect ratio and is sensitive to the constitutive relation for the bed slope effect that affects the sediment transport partitioning just upstream of the bifurcation.

The theory predicts that symmetrical bifurcations in natural rivers are unstable for low Shields stresses close to the threshold for sediment motion as often found in gravel bed rivers and for high Shields stresses in the range typically found in sand bed rivers. This means that such bifurcations develop toward an asymmetrical equilibrium configuration. On the other hand, for intermediate Shields stresses the theory predicts that bifurcations can be stable. Such conditions can perhaps be found in very low energy fluvial plains and deltas.

Our results are valid in the absence of destabilizing factors commonly found in natural rivers such as gradient advantage of a downstream branch or bars or channel curvature upstream of the bifurcation. The theory is

corroborated by field data on the asymmetry of bifurcations in sand bed rivers, laboratory data for asymmetry and stability of bifurcations in low Shields stress conditions, and numerical investigations of both gravel bed and sand bed rivers. However, there is a lack of data for stability of bifurcations in high Shields stress conditions.

Appendix A: Governing Equations, Equilibrium Configurations, and Stability

Let us consider the governing equations for the equilibrium configuration in the river bifurcation. The requirement of normal flow conditions in downstream channels can be expressed in the form

$$Q_i = b_i C_i D_i \sqrt{g D_i S_i}, \tag{A1}$$

where S_i represents the slope of channel i (b or c), b_i the channel width, C_i the dimensionless Chezy coefficient, D_i flow depth, and g gravity. Water discharge balance at the bifurcation requires

$$Q_a = Q_b + Q_c. \tag{A2}$$

We also assume the constancy of water level ($h_N = h_a = h_b = h_c$) at the bifurcation; hence, the longitudinal slope of channel i (b or c) can then be expressed in the form

$$S_i = \frac{h_N - h_i^L}{L_i}, \tag{A3}$$

where h_i^L is the free surface elevation at distance L_i downstream from the bifurcation. Exner equation applied to both cells of the final reach of channel a reads

$$\frac{q_{sb} - q_{sa}\left(\frac{b_a}{b_b+b_c}\right)}{\alpha b_a} - \frac{q_{sy}}{b_b} = 0, \tag{A4}$$

$$\frac{q_{sc} - q_{sa}\left(\frac{b_a}{b_b+b_c}\right)}{\alpha b_a} + \frac{q_{sy}}{b_c} = 0. \tag{A5}$$

Equations (A4) and (A5) can be simply manipulated to provide continuity of sediment flux at the bifurcation:

$$Q_{sa} = Q_{sb} + Q_{sc} \tag{A6}$$

and the total transverse sediment flux Q_{sy} upstream of the bifurcation:

$$Q_{sy} = \frac{1}{2}\left[Q_{sb} - Q_{sc} + Q_{sa}\left(\frac{b_c - b_c}{b_b + b_c}\right)\right]. \tag{A7}$$

The transverse water discharge Q_y at the bifurcation has to satisfy a similar continuity constraint:

$$Q_y = \frac{1}{2}\left[Q_b - Q_c + Q_a\left(\frac{b_c - b_c}{b_b + b_c}\right)\right]. \tag{A8}$$

Finally, the transverse sediment exchange between the two adjacent cells of the final reach of channel a (see Figure 1) is estimated on the basis of a well-established approach employed to describe bed load transport over an inclined bed [*Ikeda et al.*, 1981]:

$$q_{sy} = q_{sa}\left[\frac{V}{\sqrt{U^2 + V^2}} - \frac{r}{\sqrt{\vartheta_a}}\frac{\partial \eta}{\partial y}\right], \tag{A9}$$

where the transverse velocity V is evaluated through a mass balance applied to each of the two cells, the transverse bed slope $\partial\eta/\partial y$ is calculated in terms of the difference between bed elevations at the inlet of channels b and c [*Bolla Pittaluga et al.*, 2003], and the Shields number is calculated as

$$\vartheta = \frac{\rho U^2}{(\rho_s - \rho) C^2 g d_s}. \tag{A10}$$

We then have an algebraic system of nine equations in nine unknowns (D_b, S_b, Q_b, D_c, S_c, Q_c, h_N, Q_y, and Q_{sy}) that needs to be solved in order to determine the equilibrium configuration of the network. Let us consider for the sake of simplicity the simple case where the two downstream branches have the same length ($L_b = L_c$), the same width ($b_b = b_c = b_a/2$), and the same boundary conditions ($h_b^L = h_c^L$). In order to determine the threshold conditions for the appearance of multiple equilibrium configurations, we employ a perturbative approach and expand every function f in terms of a small parameter ϵ in the form

$$f = f_0 + \epsilon f_1 + \mathcal{O}(\epsilon^2)\,. \tag{A11}$$

For example, flow discharge in channel b can be expressed as $Q_b = Q_{b0} + \epsilon Q_{b1} + \mathcal{O}(\epsilon^2)$. The values attained by every function f at each order of approximation (namely, f_0 and f_1) can be obtained by considering a Taylor expansion in the neighborhood of $\epsilon = 0$ in the form

$$f(\epsilon) = f|_{\epsilon=0} + \left.\frac{\mathrm{d}f}{\mathrm{d}\epsilon}\right|_{\epsilon=0} \epsilon + \cdots. \tag{A12}$$

Equating (A11) and (A12), one immediately gets

$$f_0 = f|_{\epsilon=0}\ , \quad f_1 = \left.\frac{\mathrm{d}f}{\mathrm{d}\epsilon}\right|_{\epsilon=0}. \tag{A13}$$

By substituting such expansions (A11) in the normal flow equation (A1), in the sediment transport formula (equation (1) of the main paper) and in the nodal conditions (A2, A4, A5, and A6), we end up with a series of algebraic systems that can be solved at each order of approximation. Specifically, at leading order $\mathcal{O}(\epsilon^0)$ the trivial solution characterized by the same flow conditions in the downstream branches is found, namely, $D_{b0} = D_{c0} = D_a$, $Q_{b0} = Q_{c0} = Q_a/2$, $Q_y = Q_{sy} = 0$, $Q_{sb0} = Q_{sc0} = Q_{sa}/2$. Proceeding at first order $\mathcal{O}(\epsilon)$, the expansion of uniform flow in channel b (equation (A1)) will read

$$\frac{Q_{b1}}{Q_{b0}} = \frac{3}{2}\frac{D_{b1}}{D_{b0}} + \frac{C_{b1}}{C_{b0}} + \frac{1}{2}\frac{S_{b1}}{S_{b0}} \tag{A14}$$

and similarly in channel c with the subscript b replaced by c. Expansion of sediment transport relation in channel b (equation (1) of the main paper) will read

$$\frac{Q_{sb1}}{Q_{sb0}} = \frac{m\vartheta_{b0}}{(\vartheta_{b0} - \vartheta_{cr})}\left(\frac{D_{b1}}{D_{b0}} + \frac{S_{b1}}{S_{b0}}\right) + D_{b1}\ \frac{1}{n}\left.\frac{\mathrm{d}n}{\mathrm{d}D}\right|_{\epsilon=0}, \tag{A15}$$

where it is relevant to notice that the derivative term $\frac{\mathrm{d}n}{\mathrm{d}D}$ differs depending on the sediment transport formulations considered (n is a constant for Meyer-Peter and Müller (MPM) and a function of C for Engelund and Hansen (EH)). Expansion of the logarithmic law to evaluate the dimensionless Chezy coefficient C will read

$$C_{b0} = 6 + 2.5\log\left(\frac{D_{b0}}{2.5d_s}\right)\ , \quad C_{b1} = 2.5\frac{D_{b1}}{D_{b0}}. \tag{A16}$$

The geometrical constraints ($L_b = L_c$) and ($h_b^L = h_c^L$) will also imply that $S_{b1} = S_{c1}$. Perturbation of transverse water flux at the node will read

$$Q_{y1} = \frac{1}{2}\left(Q_{b1} - Q_{c1}\right). \tag{A17}$$

Similarly, the perturbation of the transverse sediment flux at the node will read

$$Q_{sy1} = \frac{1}{2}\left(Q_{sb1} - Q_{sc1}\right), \tag{A18}$$

but also expansion of equation (A9) will read

$$\frac{q_{sy1}}{q_{sa}} = \frac{Q_{y1}}{\alpha Q_a} - \frac{r}{\sqrt{\vartheta_a}}\frac{\left(D_{c1} - D_{b1}\right)}{0.5b_a}. \tag{A19}$$

Finally, by substituting equations (A14) and (A15) into (A2) and (A6), we get

$$\left(\frac{D_{b1}+D_{c1}}{D_a}\right)\left[\frac{D_a}{n}\frac{\mathrm{d}n}{\mathrm{d}D}\bigg|_{\epsilon=0}-\left(2+\frac{5}{C_a}\right)\frac{m\vartheta_{b0}}{(\vartheta_{b0}-\vartheta_{cr})}\right]=0. \tag{A20}$$

Also, by substituting equations (A14) and (A15) into (A17), (A18), and (A19), we get

$$\begin{aligned}\left(\frac{D_{b1}-D_{c1}}{D_a}\right)\left[\frac{1}{4}\left(\frac{3}{2}+\frac{2.5}{C_a}\right)+\frac{2r\alpha}{\beta_a\sqrt{\vartheta_a}}\right]=\\ =\left(\frac{D_{b1}-D_{c1}}{D_a}\right)\left[\frac{1}{4}\left(\frac{m\vartheta_{b0}}{(\vartheta_{b0}-\vartheta_{cr})}+\frac{D_a}{n}\frac{\mathrm{d}n}{\mathrm{d}D}\bigg|_{\epsilon=0}\right)\right].\end{aligned} \tag{A21}$$

The l.h.s. of equation (A21) represents the increase of sediment flux provided to the downstream channels from the node due to a perturbation of flow depth downstream. It is basically the ratio Q_{sy1}/Q_{sa} expressed perturbing equation (A9). The r.h.s. of equation (A21) represents the increase in sediment transport capacity of the downstream branches due to a perturbation of flow depth. We then have a homogeneous system of equations (A20 and A21) in the two unknowns $\left(D_{b1}+D_{c1}\right)/D_a$ and $\left(D_{b1}-D_{c1}\right)/D_a$. The trivial configuration $D_{b1}=D_{c1}=0$ is a solution of the system. By forcing the determinant of the matrix coefficients to vanish, we can investigate whether multiple solutions exist. Such requirement turns out to provide two equations: the first equation vanishes only in case the Chezy coefficient attains a nonphysical value, whereas the second equation is represented by equation (3) of the main paper. Such equation turns out to exactly coincide with the stability diagram of a river bifurcation derived numerically [*Bolla Pittaluga et al.*, 2003]. As such, it represents both the threshold condition for the stability of a symmetrical river bifurcation and a condition where multiple solution exists (see also Figure 3). Finally, for gravel bed rivers dominated by bed load transport, the Meyer-Peter and Müller relation applies ($n=8$, $m=1.5$), so that equation (3) of the main paper reduces to

$$\beta_a\sqrt{\vartheta_a}=8\alpha r\left[\frac{3}{2}\left(\frac{\vartheta_{cr}}{\vartheta_a-\vartheta_{cr}}\right)-\frac{2.5}{C_a}\right]^{-1}. \tag{A22}$$

In the case of sand bed rivers dominated by suspended load transport the Engelund and Hansen relation applies ($n=0.05C^2$, $m=2.5$, and $\vartheta_{cr}=0$), so that equation (3) of the main paper reduces to

$$\beta_a\sqrt{\vartheta_a}=8\alpha r\left(1+\frac{2.5}{C_a}\right)^{-1}. \tag{A23}$$

Appendix B: Bifurcations in the Cumberland Marshes

Here we briefly describe the data collected at bifurcations (Table B1) in the Cumberland Marshes, Saskatchewan River, Canada. The bifurcations used from the Columbia River [*Kleinhans et al.*, 2012] are for the sake of completeness also provided in the table and were collected with the same methods.

B1. Study Area and Data Collection

The Saskatchewan River derives its name from a Cree Indian word meaning Rapid River, referring to the braided sections. Several tens of kilometers upstream of Cumberland House, the river transformed into a highly sinuous meandering stream with cohesive banks. In this area, the river avulsed repeatedly during the past several thousands of years after the glacial lake Agassiz withdrew. The latest avulsion took place in the 1870s when the Saskatchewan River spilled into a shallow lake with a dense clay floor covered with 0.1–0.2 m resistive, detrital peat [*Smith et al.*, 1989, 1998]. Since then, the river prograded into the basin to form the Cumberland Marshes. In the upstream reach, channels formed simultaneously and were partly abandoned. In the downstream reach, the Mossy delta formed. The present-day Cumberland Lake spills back into the Saskatchewan River near Cumberland House, some 60 km downstream of the avulsion site.

In 1965 a hydropower dam was installed upstream of the avulsion site, which regulates the flow and traps most of the suspended wash load sediment and all of the transported bed sediment. The mean annual discharge released by the dam is about 500 m^3/s with most of the discharge during the week days. The guaranteed minimum discharge is 50 m^3/s. In 2005 an extremely large control flood with a peak discharge of about 2700 m^3/s flooded most of the area. The diurnal and weekly discharge fluctuations are damped out toward

Table B1. Study Site Characteristics for the Cumberland Marshes (New Data) and the Columbia River [*Kleinhans et al.*, 2012], Ordered From Upstream to Downstream[a]

Site	D	S	W_1	W_2	W_3	R_1	R_2	R_3	A_1	A_2	A_3
Cumberland Marshes											
Avulsion (Old Channel)	1000	1.0×10^{-4}	380	324	139	4.9	6.1	3.4	1900	2030	480
Steamboat	500	1.0×10^{-4}	219	25	147	7.1	0	6.8	1560	0	1000
North Angling	500	1.0×10^{-4}	173	30	152	6.2	3.8	6.3	1100	110	950
Smith1 Island	500	1.0×10^{-4}	135	113	104	5.9	5.4	2	820	660	220
Delta1	150	0.5×10^{-4}	140	164	128	4.6	2.7	1.6	610	450	220
Delta3	150	0.5×10^{-4}	124	71	49	2.2	1.3	3.1	270	100	160
Columbia River											
Bif 2	653	2.2×10^{-4}	87	37.2	30.4	2.55	2.81	2.32	225	112	74
Bif 3	762	2.2×10^{-4}	98	48.9	34.4	2.65	2.62	2.11	267	133	76
Bif 1	510	2.2×10^{-4}	54.8	31.4	55.9	2.95	1.99	2.45	165	66	141
Bif 4	725	2.2×10^{-4}	63.3	53.5	20.5	3.62	3.87	2.14	240	218	48
Bif 5	510	2.2×10^{-4}	73.3	64.6	19.4	4.33	4.63	1.24	330	315	25

[a] D = estimated mean grain size in upstream channel (in μm), S = channel slope (in m/m), W = channel width (in m), R = hydraulic radius (in m), A = cross-sectional area (in m^2), subscript 1 is for the upstream channel, 2 for the left downstream, and 3 for the right downstream of the bifurcation. All widths and depths are estimated averages from the cross-sectional and long profiles. Bifurcation names of the Columbia River are the same as in *Kleinhans et al.* [2012, Figure 2].

the downstream half of the Cumberland Marshes due to the presence of many small parallel channels, lakes, and floodplains.

Six study sites were selected (Table B1) with varying downstream branch lengths and local upstream channel planforms. Trifurcations, with three downstream branches, were avoided. Aerial photographs (N. Smith, personal communication, 2006) were available for most sites around 1945 or 1947, 1953, 1968 or 1977, and 1982 and were completed with the oblique low-altitude photographs taken on 18 July 2006 by M.G.K.

Bathymetric data were collected at cross sections upstream and downstream of most sites in 2006, except for the 1870s avulsion and steamboat sites which were sampled in 2003 and 2004. The depth was measured by a hand-held echosounder with an accuracy of 0.1 m, and the height of the banks above the water surface was visually estimated with the same accuracy. The distance to the banks was measured by a hand-held laser range finder with an accuracy of 1 m. Measurements were assisted by Norman Smith and Esther Stouthamer. The 2003 and 2004 cross sections were surveyed to benchmarks of the Watershed Authority.

To identify inlet step heights to further assess discharge asymmetry and inlet step locations to assess the representativeness of the cross sections, long sections were collected along the midchannel lines for the downstream channels, extended into the upstream channel, by drifting downstream in the boat. Water depths were measured every 15 s, while the distance to the bifurcation was measured. The boat velocity in the upstream branch was very constant at 1.2 m/s and was used to determine the sample point locations in the downstream branches.

For lack of detailed and accurate water surface elevation measurements during various conditions, the slope of the channels is largely unknown, so we take the average slope and bankfull water depths. The Saskatchewan River has a water surface slope of about 8 cm/km, but in the Cumberland Marshes the slope declines toward a few mm/km in the Mossy Delta. We estimated gradients from elevation maps and surveys in general agreement with *Edmonds and Slingerland* [2008]. Below we briefly describe the locations in the Cumberland Marshes referred to in Table B1, and data are presented with 2006 photographs for context.

B2. 1870s Avulsion Site

The last major nodal avulsion of the Saskatchewan River occurred in the 1870s [*Smith et al.*, 1989, 1998], when flood water ran through a new chute cutoff out of a sharp meander bend of the Old Channel into the Ancestral South Angling Channel, reoccupying this former course of the Saskatchewan River. Two major channels evolved: the Steamboat channel (see below) to the northeast and the Centre Angling (see below) to the east, which formed in the elongated floodplain between the North Angling Channel and the Ancestral South

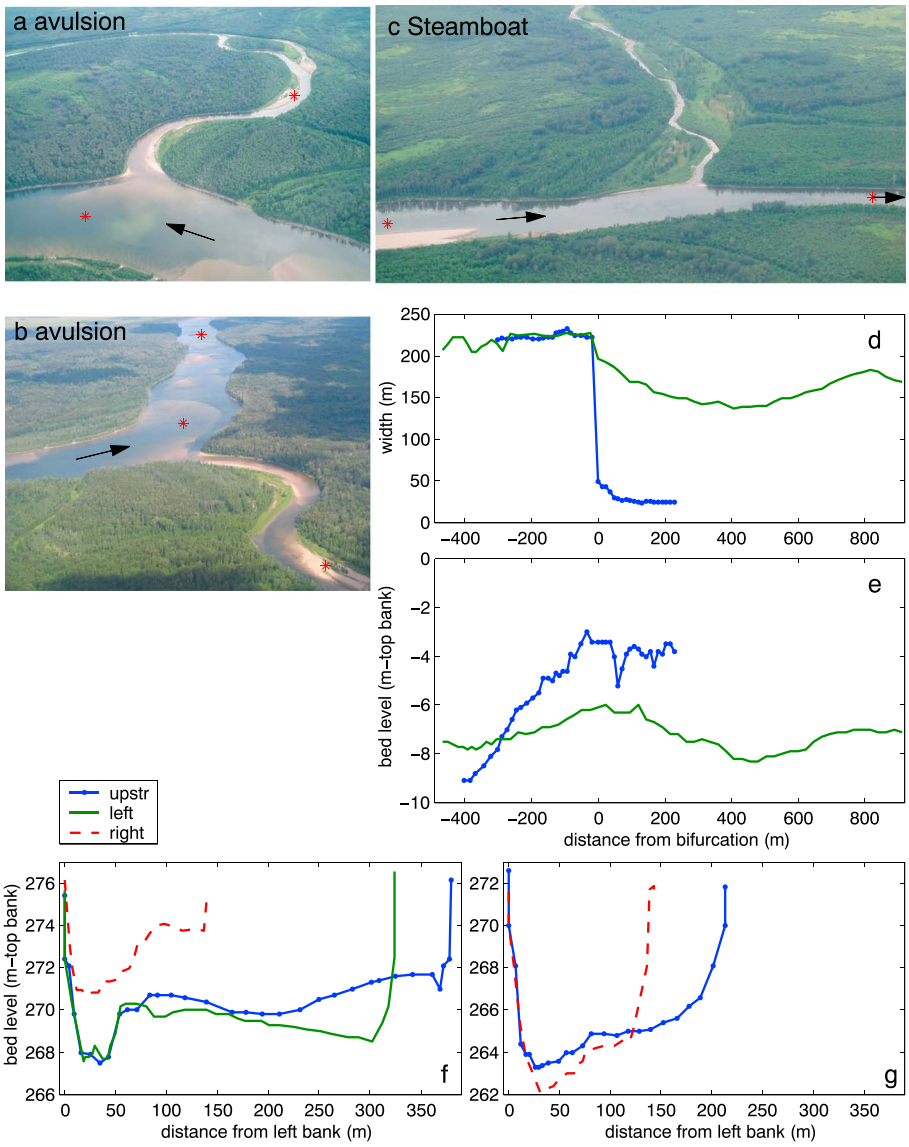

Figure B1. (a and b) The avulsion site at the Old Channel (right) and New Channel (left) and (c) the avulsion of the Steamboat channel. Arrows indicate flow direction; asterisk indicates approximate location of cross sections. (d) Widths and (e) depths at the Steamboat are given as longitudinal profiles. (f and g) Cross-sectional data for both sites were collected in 2003 and 2004. Note the scour hole just downstream of the bifurcation.

Angling Channel. Steamboats continued to use the Old Channel for about a decade, after which the New Channel and the Steamboat channels became favored [*Smith et al.*, 1998].

The aerial photographs show that the closure process of the Old Channel has presently stalled in a situation where the width and depth still are slightly less than one half of the New Channel (Figure B1), and there is a clear inlet step in the bed. The Old Channel continues to convey some of the flow and sediment attested by dunes on the bed and emergent pointbars, making it a stable asymmetrical bifurcation.

B3. Steamboat Channel

In 1945 and 1953, the Steamboat was still a wide channel and the Centre Angling was only a quarter of the width of the Steamboat. In 1977 the Centre Angling had nearly obtained its present-day width, while the Steamboat channel had silted up considerably. The Steamboat channel was filled in with sand bars for about two thirds of its length in 1982.

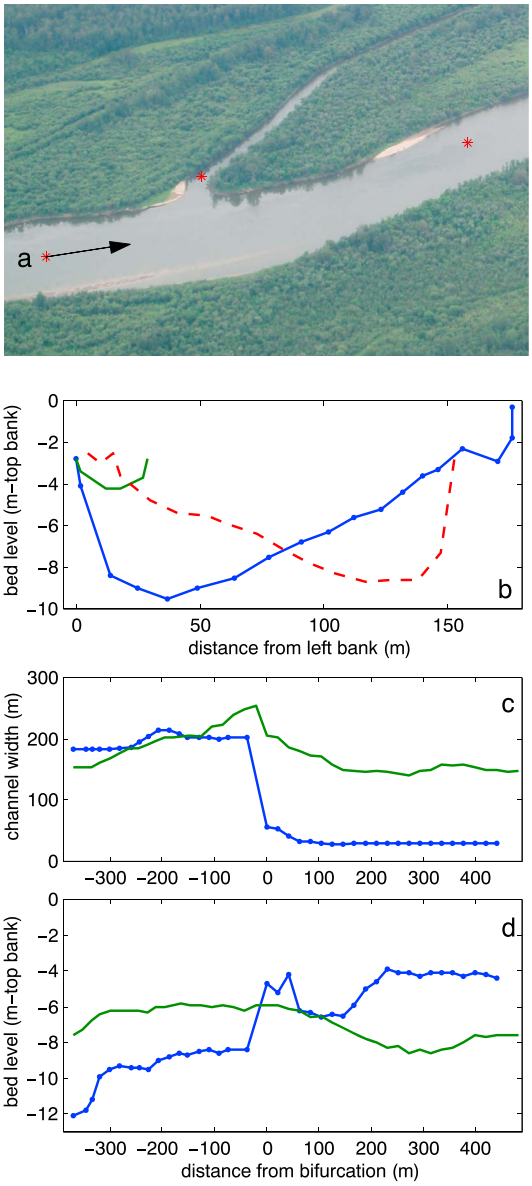

Figure B2. (a) The bifurcation of the Centre Angling and the North Angling. Note the vortex bar at the entrance of the North Angling. (b) Cross sections showing alternate bars in the large channels. (c) Measured widths along the channels. The difference in width upstream of the bifurcation is caused by including or excluding the vortex bar. (d) Bed elevation profiles along the channels showing the pronounced inlet step, the vortex bar, and the scour downstream of it.

The entrance of the Steamboat channel is presently nearly closed by a plug bar of fine sand up the height of the upstream New Channel levees. The most downstream part (before entering the Mossy River channels) is still deep, wide, and now being filled up with mud and organic detritus and has pioneer vegetation on the emergent side bars. The original channel width is still recognizable in the aerial photo (Figure B1c). The Steamboat channel only captures a small portion of the upstream discharge during formative flow events, making this site a stable, highly asymmetrical bifurcation.

B4. North and Centre Angling

In 1945 the Centre Angling flowed into the North Angling, and by 1977 most discharge had transferred to the Centre Angling (Figure B2). Meanwhile, it had widened and (nearly) closed off several of the smaller side branches along islands (see next section). The width of the North Angling Channel remained remarkably constant due to its stable, cohesive banks, and later aerial photographs show hardly any development of the Centre Angling.

The entrance of the North Angling displays an inlet step and a plug bar of about 4 m high, with a considerable scour hole just downstream of the entrance (Figure B2d), similar but much longer than in the Steamboat entrance. As the entrance is still open, the channel conveys some discharge, making this a stable, asymmetrical bifurcation.

B5. Smith Islands

Two islands developed (Figure B3a) as the Centre Angling built levees and scoured its channel. In 1945 the channels on both sides of both islands were both still open, but in 1977 the right channel of the downstream Smith2 Island was entirely dry. On the other hand, both channels around the Smith1 Island remained entirely open, although the right channel at Smith1 Island is now considerably shallower than the left channel (Figure B3b). Yet the bed is covered in large dunes, and there is a deep confluence scour just downstream of it (Figure B3c and B3e), showing that there is still significant flow through the right channel during floods. We use this case as a stable asymmetrical bifurcation, although it is not entirely clear whether the right channel at Smith1 Island could develop similarly as the Smith2 Island.

B6. Mossy Delta Bifurcations

The Mossy River Delta has tens of bifurcations and two well-defined trifurcations. From the aerial photographs it appears that about two thirds of the bifurcations have bifurcates of similar widths, and the remainder have one narrow and one wider bifurcate. However, based on visually estimated flow, bed forms, and sand cover on the bed, it appears that one channel discharges most of the water and sandy sediment. In fact, many other channels do not even have sand on the bed but show tabular cross sections with plane beds consisting

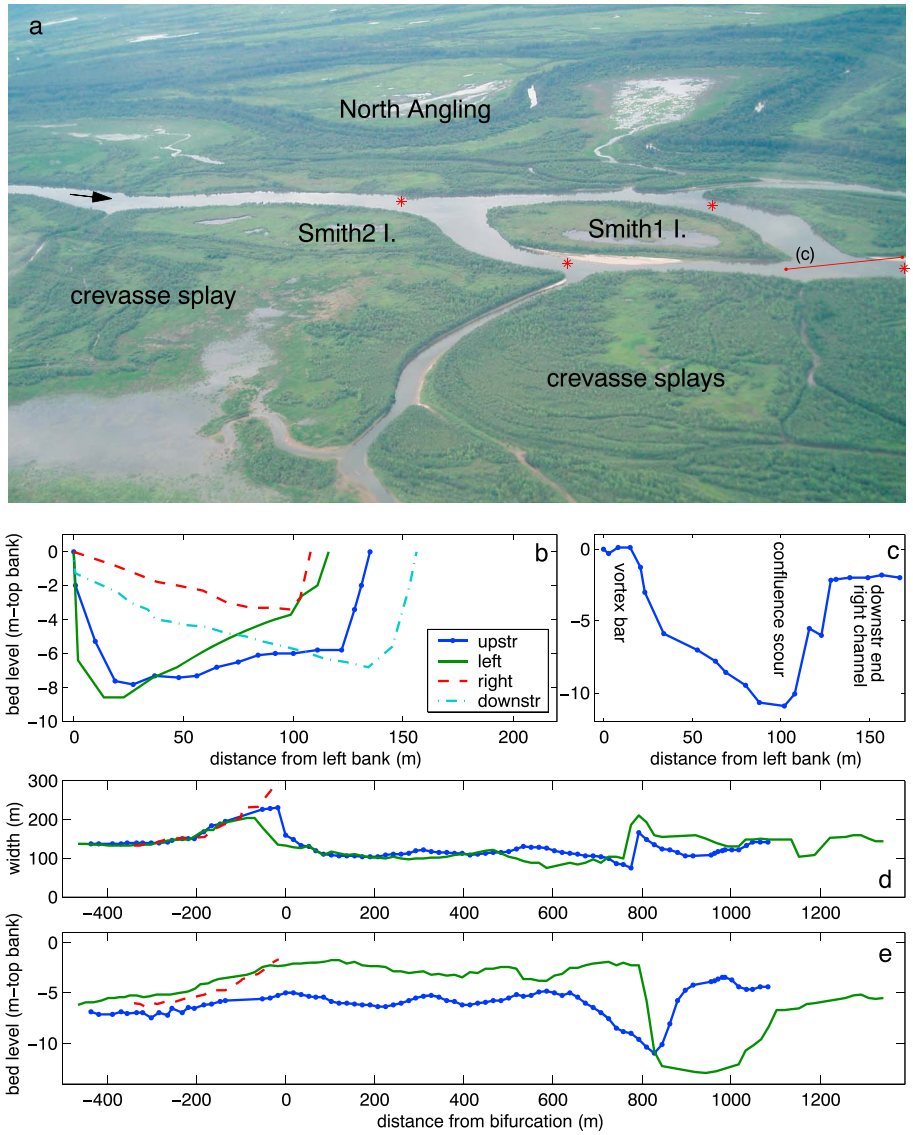

Figure B3. (a) The Smith1 Island has water on both sides, whereas the Smith2 Island has the right channel closed off. (b) The transverse bed slopes clearly indicate meandering flow. (c) Note the vortex bar, the confluence scour, and the shallowness of the right channel in the additional profile from the downstream end of the right channel into the vortex bar downstream of the confluence (location indicated in Figure B3a). (d) Variations in channel width along the channel showing widening just upstream of bifurcations and at confluences. (e) Bed elevation profiles along the channels showing a negative step just upstream of the confluence scour.

of resistive lake peat as found in soil augers. This would render modeling with sediment transport capacity (as in *Edmonds and Slingerland* [2008]) invalid. We therefore only selected the first bifurcation, which is fully alluviated, and the third bifurcation on the left side of the delta, which is at least partly alluviated (Figure B4).

According to the aerial photographs and as verified in site visits, the delta bifurcations formed following a well-known pattern: a V-shaped midchannel bar of silty sediment covered in vegetation forms where the upstream channel debouches into the lake. While prograding, two new channels form at the sides of the V-shaped bar. In 1947 the first bifurcation had fully formed as well as some asymmetrical bifurcations. In 1953 fourth bifurcations were forming, and in 1968 and 1982 the delta had again extended considerably. Until 1968 the main discharge seems to have flowed left, left, left, and left, but in 1982 a rather straight channel directly into the Cumberland Lake without further bifurcations had formed (left, right, and left), which remains the

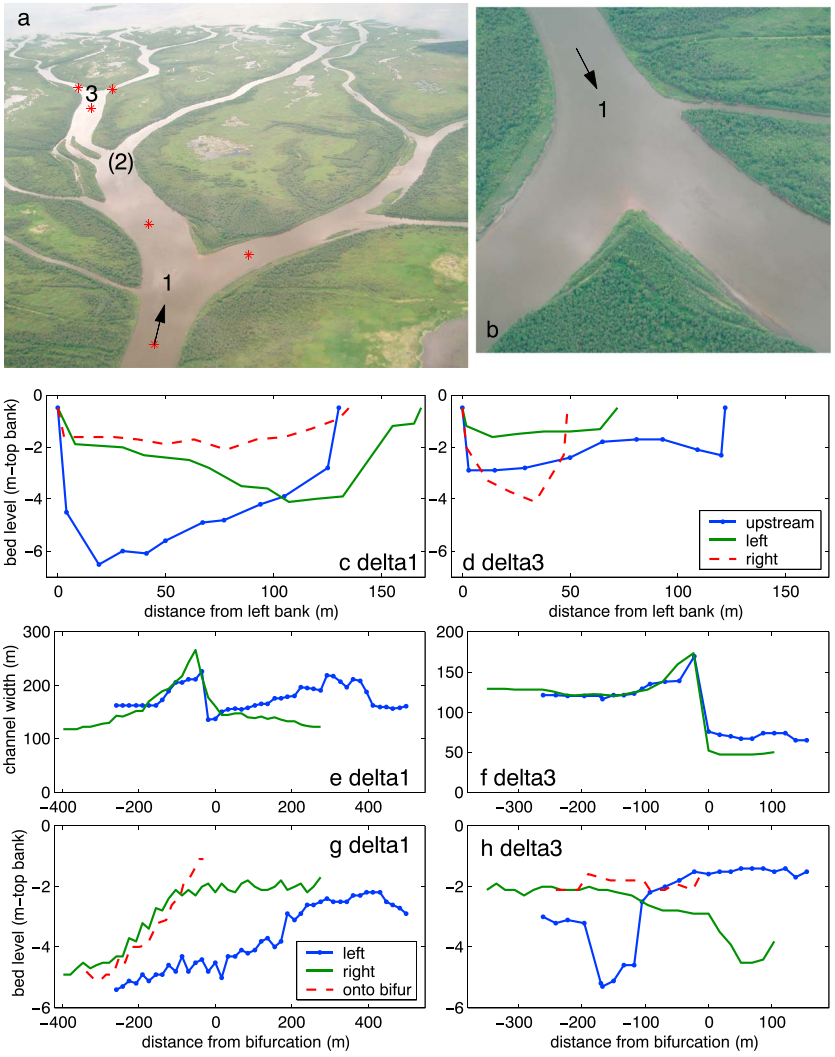

Figure B4. Bifurcations in the Mossy delta. Data were collected at the first and third bifurcations. The third had (d) an upstream midchannel bar with most of the flow on the left side, which crossed over to the right channel at the bifurcation through a narrow deep channel visible in the left long section. The trifurcations are on the left and right of the photographed area.

main channel until today. In 2006 the delta had not extended much farther than in 1982. This is perhaps an effect of the sediment trapping at the dam, preventing further progradation of the levees. We use both cases as stable, asymmetrical bifurcations.

Acknowledgments

G.C. acknowledges funding from the AGL Programme. M.G.K. was supported by the Netherlands Organisation for Scientific Research (NWO), grant ALW-Vidi-864.08.007. M.G.K. acknowledges Norman Smith for his hospitality and help in the field (Cumberland Marshes). The data reported in the figures can be made available at request by the corresponding author (M. Bolla Pittaluga).

The Editor thanks Rudy Slingerland and an anonymous reviewer for their assistance in evaluating this paper.

References

Bertoldi, W., and M. Tubino (2007), River bifurcations: Experimental observations on equilibrium configurations, *Water Resour. Res.*, *43*, W10437, doi:10.1029/2007WR005907.

Bolla Pittaluga, M., R. Repetto, and M. Tubino (2003), Channel bifurcation in braided rivers: Equilibrium configurations and stability, *Water Resour. Res.*, *39*(3), 1046, doi:10.1029/2001WR001112.

Bolla Pittaluga, M., R. Luchi, and G. Seminara (2014), On the equilibrium profile of river beds, *J. Geophys. Res. Earth Surf.*, *119*, 317–332, doi:10.1002/2013JF002806.

Edmonds, D. A., and R. L. Slingerland (2008), Stability of delta distributary networks and their bifurcations, *Water Resour. Res.*, *44*, W09426, doi:10.1029/2008WR006992.

Edmonds, D. A., R. L. Slingerland, J. Best, D. Parsons, and N. Smith (2010), Response of river-dominated delta channel networks to permanent changes in river discharge, *Geophys. Res. Lett.*, *37*, L12404, doi:10.1029/2010GL043269.

Engelund, F., and E. Hansen (1967), *A Monograph on Sediment Transport in Alluvial Streams*, Tech. Univ. of Denmark, Technisk Forlag, Copenhagen, Denmark.

Ikeda, S., G. Parker, and K. Sawai (1981), Bend theory of river meanders. Part 1. Linear development, *J. Fluid Mech.*, *112*, 363–377.

Kleinhans, M. G., and J. H. van den Berg (2011), River channel and bar patterns explained and predicted by an empirical and a physics-based method, *Earth Surf. Processes Landforms*, *36*, 721–738, doi:10.1002/esp.2090.

Kleinhans, M. G., H. R. A. Jagers, E. Mosselman, and C. J. Sloff (2008), Bifurcation dynamics and avulsion duration in meandering rivers by one-dimensional and three-dimensional models, *Water Resour. Res.*, *44*, W085454, doi:10.1029/2007WR005912.

Kleinhans, M. G., H. J. T. Weerts, and K. M. Cohen (2010), Avulsion in action: Reconstruction and modelling sedimentation pace and upstream flood water levels following a Medieval tidal-river diversion catastrophe (Biesbosch, The Netherlands, 1421–1750 AD), *Geomorphology*, *118*, 65–79, doi:10.1016/j.geomorph.2009.12.009.

Kleinhans, M. G., K. M. H. Cohen, J. Hoekstra, and J. M. IJmker (2011), Evolution of a bifurcation in a meandering river with adjustable channel widths, Rhine delta apex, The Netherlands, *Earth Surf. Processes Landforms*, *36*, 2011–2027.

Kleinhans, M. G., T. de Haas, E. Lavooi, and B. Makaske (2012), Network dynamics and origin of anastomosis in the upper Columbia River, Canada, *Earth Surf. Processes Landforms*, *37*, 1337–1351, doi:10.1002/esp.3282.

Kleinhans, M. G., R. I. Ferguson, S. N. Lane, and R. J. Hardy (2013), Splitting rivers at their seams: Bifurcations and avulsion, *Earth Surf. Processes Landforms*, *38*, 47–61, doi:10.1002/esp.3268.

Makaske, B. (2001), Anastomosing rivers: A review of their classification, origin and sedimentary products, *Earth Sci. Rev.*, *53*, 149–196.

Meyer-Peter, E., and R. Müller (1948), Formulas for bedload transport, paper presented at 2nd Meeting of International Association for Hydraulic Research, Stockholm, Sweden.

Miori, S., R. Repetto, and M. Tubino (2006), A one-dimensional model of bifurcations in gravel bed channels with erodible banks, *Water Resour. Res.*, *42*, W11413, doi:10.1029/2006WR004863.

Miori, S., R. J. Hardy, and N. Lane (2012), Topographic forcing of flow partition and flow structures at river bifurcations, *Earth Surf. Processes Landforms*, *37*, 666–679.

Slingerland, R., and N. D. Smith (1998), Necessary condition for a meandering-river avulsion, *Geology*, *26*(5), 435–438.

Slingerland, R., and N. Smith (2004), River avulsions and their deposits, *Annu. Rev. Earth Planet. Sci.*, *32*, 257–285.

Sloff, K., and E. Mosselman (2012), Bifurcation modelling in a meandering gravel-sand bed river, *Earth Surf. Processes Landforms*, *37*, 1556–1566.

Smith, N. D., T. A. Cross, J. P. Dufficy, and S. R. Clough (1989), Anatomy of an avulsion, *Sedimentology*, *36*, 1–23.

Smith, N. D., R. L. Slingerland, M. Pérez-Arlucea, and G. S. Morozova (1998), The 1870's avulsion of the Saskatchewan River, *Can. J. Earth Sci.*, *35*(4), 453–466.

Syvitski, J. P. M., and Y. Saito (2007), Morphodynamics of deltas under the influence of humans, *Global Planet. Change*, *57*, 261–282.

van der Mark, C. F., and E. Mosselman (2013), Effects of helical flow in one-dimensional modelling of sediment distribution at river bifurcations, *Earth Surf. Processes Landforms*, *38*, 502–511.

van Rijn, L. C. (1984), Sediment transport, Part II: Suspended load transport, *J. Hydraul. Eng.*, *110*(11), 1431–1456.

Wang, Z. B., R. J. Fokkink, M. De Vries, and A. Langerak (1995), Stability of river bifurcations in 1D morphodynamics models, *J. Hydraul. Res.*, *33*(6), 739–750.